General Disclaimer

One or more of the Following Statements may affect this Document

- This document has been reproduced from the best copy furnished by the organizational source. It is being released in the interest of making available as much information as possible.

- This document may contain data, which exceeds the sheet parameters. It was furnished in this condition by the organizational source and is the best copy available.

- This document may contain tone-on-tone or color graphs, charts and/or pictures, which have been reproduced in black and white.

- This document is paginated as submitted by the original source.

- Portions of this document are not fully legible due to the historical nature of some of the material. However, it is the best reproduction available from the original submission.

NASA TECHNICAL MEMORANDUM

NASA TM-73770

NASA TM-73770

PARAMETRIC DEPENDENCE OF ION TEMPERATURE AND RELATIVE DENSITY IN THE NASA LEWIS SUMMA FACILITY

by A. Snyder, M. R. Lauver, and R. W. Patch
Lewis Research Center
Cleveland, Ohio 44135

TECHNICAL PAPER presented at the
Eighteenth Annual Meeting on Plasma Physics
sponsored by the American Physical Society
San Francisco, California, November 14-18, 1976

PARAMETRIC DEPENDENCE OF ION TEMPERATURE AND RELATIVE DENSITY IN THE NASA LEWIS SUMMA FACILITY

by A. Snyder, M. R. Lauver, and R. W. Patch

National Aeronautics and Space Administration
Lewis Research Center
Cleveland, Ohio 44135

ABSTRACT

Further hot-ion plasma experiments were conducted in the SUMMA superconducting magnetic mirror facility. A steady-state $\overline{E}x\overline{B}$ plasma was formed by applying a strong radially inward dc electric field between cylindrical anodes and hollow cathodes located near the magnetic mirror maxima. Extending the use of water cooling to the hollow cathodes, in addition to the anodes, resulted in higher maximum power input to the plasma. Steady-state hydrogen plasmas with ion kinetic temperatures as high as 830 eV were produced. Functional relations were obtained empirically among the plasma current, voltage, magnetic flux density, ion temperature, and relative ion density. The functional relations were deduced by use of a multiple correlation analysis. Data were obtained for midplane magnetic fields from 0.5 to 3.37 tesla and input power up to 45 kW. Also, initial absolute electron density measurements are reported from a 90° Thomson scattering laser system.

E-9563

PARAMETRIC DEPENDENCE OF ION TEMPERATURE AND RELATIVE DENSITY IN THE NASA LEWIS SUMMA FACILITY

by A. Snyder, M. R. Lauver, and R. W. Patch

Lewis Research Center

SUMMARY

Further hot-ion plasma experiments were conducted in the NASA Lewis SUMMA facility. A steady-state plasma discharge was formed by applying a radially inward dc electric field of several kilovolts near the magnetic mirror maxima. Results are reported for a hydrogen plasma covering a wide range in midplane magnetic flux densities from 0.5 to 3.37 tesla. Input power greater than 45 kW was obtained with water-cooled cathodes. Steady-state plasmas with ion kinetic temperatures from 18 to 830 eV were produced and measured spectroscopically. The functional dependence among the plasma current, electrode voltage, midplane magnetic flux density, ion temperature, and relative ion density were determined using a multiple regression analysis. The most satisfactory correlations were obtained by correlating ion temperature and relative ion density with current, voltage, and magnetic flux density as the independent variables. Preliminary absolute electron density measurements were made using a laser Thomson scattering apparatus. The measured electron densities ranged from 2.1×10^{11} to 6.8×10^{12} $1/cm^3$.

E-9563

INTRODUCTION

This report presents additional results of hot-ion plasma experiments in the Superconducting Magnetic Mirror Apparatus (SUMMA) at the NASA Lewis Research Center (LeRC) (refs. 1 to 3). SUMMA has two pairs of solenoidal magnet modules serving as mirrors for plasma fusion studies. For this report only the two inboard magnet modules were used. The maximum magnetic flux density was 5.0 tesla at the mirrors, and the mirror ratio was 1.48. A steady-state plasma was formed by applying a radially inward dc electric field of several kilovolts per centimeter to water cooled electrodes near the throats of the mirrors. The mutually perpendicular electric and magnetic fields cause the electrons and ions of the plasma to drift azimuthally, in the $\bar{E}x\bar{B}$ direction. The drift velocity corresponds to an ion energy as high as several kilovolts. In previous experiments conducted in SUMMA with this plasma heating method, ion temperatures of about 1 keV were obtained with hydrogen gas (refs. 2 to 4).

This report presents the results of a study of the effect of the independent parameters of gas flow (or electric current), voltage, and magnetic field strength on ion temperature and relative ion density. The ion temperatures and relative densities were derived from Doppler-

broadened optical monochromator data taken along a diameter of the plasma beam.

For the first time at Lewis, ion temperatures and relative ion densities are reported for the low resistance plasma mode as well as the high mode. A single power law of current, voltage, and magnetic field strength (IVB) correlated all of the temperatures and another correlated all of the densities. A few electron temperatures (not previously reported) were obtained in the similar Lewis mirror apparatus HIP-1. They are presented, without IVB correlation, to reveal that the two plasma modes may have different electron heating mechanisms.

The first determinations of absolute ion density in SUMMA by a Thompson scattering laser apparatus are presented.

All of the electrodes were water-cooled for the first time in SUMMA - previously the cathodes had been uncooled. As a result, the plasma was reproducible for periods of minutes at 20 kW or more of input power.

All data were taken with hydrogen with a single configuration of water-cooled electrodes.

APPARATUS

The SUMMA facility was constructed at NASA Lewis Research Center to develop a source of hot-ion plasma for thermonuclear research use. The facility is operated from an adjacent control room. The magnets and test section have been previously described (refs. 1 to 4).

Plasma Test Section

A schematic view of the plasma test section and magnets is shown as figure 1. The test section or discharge chamber is a cylinder 3.75 m in length and 36.6 cm in diameter. The walls and ends are made from type 304 stainless steel. Two 25.4 cm diffusion pumps provide a base pressure of 5×10^{-7} torr.

Facility Instrumentation

A pressure regulator and two remotely operated variable leak valves control the mass flow rates to the two hollow cathodes. The inlet gas flow meters are read remotely in the control room.

A schematic of the high voltage circuit to the electrodes is given in figure 2. The primary power supplies were in series. They were operated up to 22 kV. The high voltage vacuum on-off switch was operated remotely from the control room. High-voltage-isolated dc current sensors

measured the cathode currents and displayed their values in the control room.

Electrode Assembly

The electrode geometry is shown schematically in figure 1. A photograph of the cathode assembly after use is presented in figure 3. A thin coating of sputtered metal can be seen covering all parts. The coating has the Cr, Ni, Fe composition of the type 304 stainless steel of the chamber walls. The electrical resistance of the film-covered insulators to ground was megohms even after tens of hours of operation. A schematic of the electrode configuration showing the location of magnetic field lines is given as figure 4. The midplane of the water-cooled anodes were located at the mirror throats. The cathode tips were outside the mirrors, 7.6 cm from the anode midplane.

Hydrogen gas flowed along the axis of the cathodes, producing a hollow cathode discharge. The boron nitride shields served as uncooled refractory electrical insulators to reduce arcing along magnetic field lines between cathode and ground points. The water-cooled floating plate protected the end walls from bombardment by fast ions and fast neutrals. A bell-shaped protector over the vacuum seal and electrical insulating porcelain gland reduced the electrical and thermal stress on the gland. The bell also shielded the porcelain from deposition of sputtered metal.

The water-cooled electrodes are the same as those previously used in Lewis' Hot Ion Plasma magnetic mirror facility (HIP-1) (refs. 3 to 5). HIP-1 has copper magnet windings, a mirror ratio of 1.82 and a maximum continuous magnetic flux density of about 2.15 T at the mirrors. The test section is similar to SUMMA's and the $\vec{E}\times\vec{B}$ method of plasma production is the same in each. The electrodes, with slight dimensional modifications, are interchangeable between the two facilities.

The water-cooled electrodes, except for the stainless steel cathode stems, were fabricated of copper. To minimize sputtering from their surfaces, those exposed to energetic plasma were coated with tungsten by a commercial plasma flame spraying process. The water-cooled floating plates and the uncooled stainless steel bell protectors for the ceramic glands were also coated with flame-sprayed tungsten.

PLASMA DIAGNOSTICS

Optical Spectroscopic Diagnostics

Experimental arrangement. - The emission spectroscopy apparatus for determining ion temperature and relative ion density is shown in figure 5. It was located at the test-section midplane and viewed the plasma perpendicular to the magnet axis. The vertical centerplane (defined as a ver-

tical plane containing the magnet axis) was focused on the entrance slit of the monochromator with a lens. Between the lens and the entrance slit the beam was rotated 90° with a beam rotator consisting of a Pechan prism. A stop was provided to reduce the vertical height of the beam. The beam cross-section at the vertical centerplane was determined by the size and shape of the entrance slit. At this point the beam cross section was approximately 2 mm in the vertical direction and 26 mm parallel to the magnet axis. An adjustable screw at the base of the monochromator stand was used to make vertical scans (fig. 5). For the work reported here the monochromator was focused across the centerline of the plasma so the quantity y in figure 5 was zero. The grating monochromator employed an f/8.6 1/2 m Ebert mounting with curved slits. The reciprocal linear dispersion was 1.6 nm/mm in first order. A photomultiplier with extended S-20 photocathode was used for detection. It was magnetically shielded and cooled with air that came from a vortex tube refrigerator.

Four hundred thirty five ion temperature data points were acquired over a 29-day period. The test section window acquired a slight coating from the plasma operation, but there was no indication that the temperature deduced from light transmitted through the window was altered. The calculated relative average ion densities, however, were more dependent on the total light transmitted through the window. Therefore, these densities were calculated only for the last 8 days (277 data points), after a shutter had been installed to minimize window deposits.

Ion temperature determination. - Observations of the Doppler-broadened Balmer H_α line emission were used to obtain a diametrical average of the ion temperature at the midplane. Figure 6 shows a typical H_α line profile taken in SUMMA. There is an intense narrow component due to electronic excitation of cold and Franck-Condon neutrals. The wide component was assumed to be due primarily to simultaneous electronic excitation and charge exchange by the reaction

$$H_f^+ + H_2 \rightarrow H_f(n = 3) + H_2^+ \qquad (I)$$

where the subscript f stands for "fast" and n is the principal quantum number. The emission spectrum from $H_f(n = 3)$ is Doppler broadened because the H_f has essentially the same velocity as H_f^+. Hence the width (or second moment) of the wide component of the H_α line was used to obtain the H_f^+ ion temperature averaged across the midplane diameter. The ion temperatures were obtained by the methods described in reference 6, where it was assumed that reaction (I) predominates. Reaction (I) will predominate if the plasma is small in size and has a low enough electron density (roughly 10^{12} cm^{-3} for a 5 cm diameter plasma), and if the following reactions can be neglected.

$$H_f^+ + H \rightarrow H_f(n = 3) + H^+ \qquad (II)$$

$$H_{2f}^{+} + H_2 \rightarrow H_f(n = 3) + H(n = 1) + H_2^{+} \qquad \text{(III)}$$

$$H_{2f}^{+} + H \rightarrow H_f(n = 3) + H_2^{+} \qquad \text{(IV)}$$

Reactions (II) and (IV) can be neglected if the degree of dissociation of H_2 to H is small. In the present experiment H_2 is fed in at the cathodes and is also created by recombination on the metal walls. Approximate calculations showed that the mean free path for the disappearance of H_2 was the same order of magnitude as the plasma radius. Since H_2 originates both at the cathodes and at the walls, it was assumed that the degree of dissociation to H was small. Reaction (III) can be neglected if the number density of H_2^{+} is much less than the number density of H^{+} (Reaction III has a larger cross section than reaction I (ref. 7)). Both the neutral particle spectrometer results (refs. 8 and 2) and an approximate composition calculation indicate that H_2^{+} is present in this type of plasma. The H_2^{+} density was estimated to be less than 15 percent of the H^{+} density. This estimate resulted from a quasi-steady state analysis which took into account six reaction rates for the production and destruction of H_2^{+}. The neglect of reaction (III) was not investigated further.

The ion temperature is dependent on ion drift via the line profiles. However, no allowance was made for ion drift in determining the ion temperatures since no drift or probe data were available. Consequently, the ion temperatures are estimated to contain an error of about ±20 percent standard deviation (refs. 4, 9 to 11).

Relative ion density determination. - The wide component of the H_α line is also useful for estimating relative ion density N averaged across a diameter at the midplane. In reference 5 it is shown that

$$N \sim \frac{A}{G\langle \sigma v \rangle} \qquad (1)$$

where A is the area of the wide component on a graph such as figure 6, G is the gas flow rate (assumed proportional to the neutral number density, σ is the optical charge-exchange cross section for H_α, v is ion velocity, and $\langle\ \rangle$ means to take an average over velocity space. The quantity $\langle \sigma v \rangle$ depends only on ion temperature and was calculated using cross sections for reaction (I) (ref. 5).

Thomson Scattering Diagnostics

Experimental arrangement. - A laser Thomson scattering system was employed to measure the absolute electron density at the center of the plasma.

Figure 7 shows the arrangement for the scattering diagnostic components. Light from a 10 joule q-switched laser with a maximum repetition rate of one shot per minute is passed through a vacuum aperture stop to remove uncollimated rays and then, using an 84 cm focal length lens, focused to an approximately 3 cm diameter spot at the intersection of the test section's axis and midplane. The laser light is polarized with its E vector parallel to the test section's axis. Laser light, scattered from the free electrons in the plasma, is collected at 90° to the incident light using either a 0.007 or a 0.12 steradian solid angle viewing system. Figure 7 shows the 0.007 steradian viewing system. This light collection optics system consists of a pair of doublet lenses, a field stop, and a third lens positioned as to give a 2.2 cm diameter parallel beam of light to a single photomultiplier (PM) tube placed behind a wide band transmission filter. The 0.12 steradian optics is similar except that the pair of doublet lenses is replaced. All PM tubes, used in this diagnostic, are EMI type 9658R. The filter has 46 nm full width at half maximum centered at 694 nm wavelength.

The primary laser beam is allowed to enter a dump relying on light absorption into sheets of black glass positioned successively at Brewster's angle with respect to the axially polarized laser light. The beam dump is shown for illustration purpose in figure 7 rotated 90° from its actual orientation. The entrance and exit ports for the primary laser path are both completely blackened and baffled. Baffling of the viewing port is similarly necessary to reduce the amount of stray light reflecting off inhomogeneities in the viewing lens and entering the collection solid angle. Opposite the viewing optics is a viewing dump port designed to provide a dark background. The viewing dump port was baffled only when employing the 0.007 steradian viewing lens.

Positioned above the beam dump is a 25 cm diameter integrating sphere which collects laser light passed through the initial sheet of black glass. A PM tube mounted to the side of the integrating sphere monitors a portion of this averaged light. The signal from both the scattered light detection PM tube and the monitor PM tube go to separate channels of a type 555 Tektronix dual beam oscilloscope. The signal traces are stored on high speed film.

The PM tubes' electronics circuit governing the dynode voltages are designed to insure linear output. A resistive tap switch circuit allows independent application of voltage to each PM tube to maintain operation in the linear range while using a single power supply. The complete electronics system was designed and installed having a single point ground. The PM tubes are shielded against magnetic flux by placing them inside pairs of concentric cylinders. The inner cylinder is made of 0.1 cm wall μ-metal and the outer of 0.64 cm wall mild-steel pipe. Not shown in figure 7 are mechanical shutters placed immediately before the entrance lens, viewing lens, and beam dump preventing unnecessary exposure to the plasma environment.

Calibration. - Absolute calibration of the Thomson scattering system to determine electron density is obtained from Rayleigh scattering in dry nitrogen. Figure 8 shows a calibration determined in this manner using the 0.12 steradian viewing lens. Each data point is an average of five shots. This calibration was made immediately before making Thomson scattering measurements. The Rayleigh differential scattering cross section for nitrogen (ref. 16) is 2.12×10^{-28} cm/sr.

Figure 8 indicates a stray light background equal to a Rayleigh scattered signal from 32 millitorr of nitrogen which is equivalent to a plasma free-electron density of $3\times10^{12}/cm^3$. In addition to the initial calibration, zero pressure ($<10^{-7}$ torr) data points were made periodically while taking Thomson scattering data to monitor changes in background stray light. Variation in the median stray light level over a day's run was undetectable, with a shot to shot variation of about 10 percent.

Figure 9 shows a calibration using the 0.007 steradian viewing lens. Each data point is for a single shot. This calibration indicates essentially no stray light. Similar calibrations are made at each photomultiplier voltage.

The filter rejection was not taken into account for the density measurement. This was calculated to be less than 5 percent for electron temperatures below 35 eV. Electron temperatures of $\leq$35 eV were assumed from previous data in SUMMA using the helium line ratio technique (ref. 6).

Electron density determination. - The theory of light scattering in plasmas is well known (ref. 12). The Thomson scattering characteristics are determined by the choice of scattering angle (θ), wavelength of incident laser radiation (λ_o), plasma electron density (n_e), and electron temperature (T_e). The pertinent characteristic parameter α is defined in reference 12 as

$$\alpha = \frac{\lambda_o}{4\pi\ \lambda_D \sin\frac{1}{2}\theta} \tag{2}$$

where λ_D is the Debye length given as

$$\lambda_D = 7.43\times10^2 \left(\frac{T_e}{n_e}\right)^{1/2} \tag{3}$$

The SUMMA plasma electron temperature and density can be considered as being 35 eV and 1×10^{13} $1/cm^3$, respectively, for representative calculation of α. This gives $\alpha = 0.033$ which can be considered much smaller than unity. For the case $\alpha \ll 1$, the motions of the free electrons in the plasma are independent and result in uncorrelated scattering. The total scattered light intensity, I_{TH}, is then directly proportional to

the number of scatterers (i.e., free electrons in the plasma) and can be expressed as

$$I_{TH} = K_{TH}\left(\frac{d\sigma}{d\Omega}\right)_{TH} n_e \tag{4}$$

where K_{TH} is the proportionality constant depending on the total incident radiation power, the scattering length, and the scattering solid angle. The quantity $(d\sigma/d\Omega)_{TH}$ is the differential Thomson scattering cross section equal to 7.94×10^{-26} cm^2/SR for 90° scattering. Since Rayleigh scattering has the same radiation characteristics as Thomson scattering, we have

$$I_R = K_R\left(\frac{d\sigma}{d\Omega}\right)_R n_R \tag{5}$$

where $(d\sigma/d\Omega)_R$ is the Rayleigh differential scattering cross section, and n_R is the number of gas molecules per cubic centimeter. The quantity K_R is the proportionality constant. Since the scattering length and solid angle are the same and if we normalize both the Rayleigh and Thomson laser pulses with respect to the monitor signal, we can write the electron density as

$$n_e = \frac{I_{TH}}{I_R} \frac{n_R\left(\frac{d\sigma}{d\Omega}\right)_R}{\left(\frac{d\sigma}{d\Omega}\right)_{TH}} \tag{6}$$

The ratio of the differential cross sections can be calculated from their known values. As was mentioned in the section on the experimental arrangement, the detection system measured the integrated scattered light intensity and produced a linear output. The ratio of the intensities is obtained by relating the Rayleigh measurements to the electron density measurements after first subtracting off the stray light contribution. The stray light level is readily obtained as shown in the calibration section. The gas pressure used for the Rayleigh scattering is measured with an accurate secondary standard pressure gage. The electron density is then determined from equation (6).

DISCUSSION OF RESULTS

Functional Dependence Among Plasma Variables

The functional dependence among the plasma variables current I, electrode voltage V, midplane magnetic flux density B, ion temperature T, and relative ion density N was investigated using spectroscopic diagnostics (for T and N) over a wider range of variables than previously

(refs. 4 and 5). In particular, B was varied over the much wider range of 0.50 to 3.40 T. The number of runs was also much larger (435).

Range of variables and general method. - For ion temperature 435 runs were made. The range of variables covered is given in table I. The last 277 of the 435 runs were also used for relative ion density (the monochrometer shutter, fig. 5, was installed for these last runs). The range of variables covered in the last 277 runs is given in table II. The values of I were dictated by discharge stability considerations: runs were only recorded for stable operating modes.

A multiple regression analysis (refs. 13 and 14) was used just as in reference 4. The correlations of T and N with G, V, and B as independent variables were not satisfactory. Much better correlations were obtained by correlating T and N with I, V, and B as independent variables. The cause of this was unclear, but there may have been variable outgassing of electrodes, shutters, or the test section.

Four-term correlations. - An appropriate form for four-term correlations was established in reference 5 as

$$D = CI^{b_1} V^{b_2} B^{b_3} \tag{7}$$

where D is any dependent variable, and C, b_1, b_2, and b_3 are constants. Taking the logarithm to the base of 10 of both sides of equation (7) gives

$$\log D = b_0 + b_1 \log I + b_2 \log V + b_3 \log B \tag{8}$$

where $b_0 = \log C$. The superiority of equation (8) over the form

$$D = b_0 + b_1 I + b_2 V + b_3 B \tag{9}$$

was confirmed in the present work. Using equation (8) as the regression equation but converting the results back to equation (7) gives for ion temperature

$$T_c = 10^{0.81\pm0.04}\, I^{0.27\pm0.02}\, V^{1.53\pm0.03}\, B^{-1.05\pm0.03} \tag{10}$$

where the tolerances are the standard deviations of the regression coefficients, and the subscript c stands for "calculated." In figure 10 the calculated ion temperature equation (10) is plotted along the abscissa, while observed temperatures are plotted along with ordinate. For a perfect fit, all the points would fall along the 45° line.

The exponents in equation (10) are compared with previous investigations in table III. Differences in b_1 and b_2 are probably due prin-

cipally to differences in mirror ratios and electrode geometry. The wide variations in b_3 are due to ion temperature not being proportional to a power of B for a wide range of B values as will be shown in the next section (previous investigations covered narrow ranges of B values).

Equation (8) was used for relative ion density (obtained from eq. (1)) in the same manner as for ion temperature. The result was

$$N_c = 10^{9.66\pm0.20}\ I^{1.26\pm0.13}\ V^{-6.92\pm0.17}\ B^{5.45\pm0.16} \qquad (11)$$

for the range of B values from 0.84 to 3.37 T (see table II). The power of 10 is not significant because N_c is relative. Observed against calculated values of N are plotted in figure 11. The correlation does not appear good even on a logarithmic scale.

A comparison of the exponents in equation (11) with a previous investigation is given in table IV. The agreement is poor. This may be partly due to the differences in mirror ratios and geometries, but is probably principally due to the different ranges of I, V, R covered. The calculations of N are based on assumptions of a small plasma diameter and low electron density which allow equation (I) to dominate the light emission process in the plasma. The plasma diameter is visibly many times larger in the low resistance mode than in the high resistance mode. Also, the relative density data are based on the integrated intensity of a line along the plasma diameter. Both the method of calculating N and the way the spectroscopic observations were made limit the application of an IVB fit to relative ion density data.

Multi-term correlations. - The difficulties in the four-term correlations were overcome and the correlations greatly improved by using multi-term correlations of the form

$$\begin{aligned}\log D = {} & b_0 + b_1 \log I + b_2 \log V + b_3 \log B \\ & + b_4 \log V \log B + b_5 \log I \log B + b_6 \log I \log V \\ & + b_7(\log I)^2 + b_8(\log V)^2 + b_9(\log B)^2 + b_{10} \log I \log V \log B \\ & + b_{11}(\log I)^2 \log V + b_{12}(\log I)^2 \log B + b_{13} \log I(\log V)^2 \\ & + b_{14}(\log V)^2 \log B + b_{15} \log I(\log B)^2 + b_{16} \log V(\log B)^2 \\ & + b_{17}(\log I)^3 + b_{18}(\log V)^3 + b_{19}(\log B)^3\end{aligned} \qquad (12)$$

where all logarithms are to the base 10. Equation (12) is the most general equation with terms up to third order. For each correlation, terms except the first that were not statistically significant were discarded by the backward elimination procedure (ref. 14). The results for D equal to T and N, are given in table V. A dash indicates that the corresponding term was discarded.

The 14-term ion temperature correlation is shown in figure 12. Here the abscissa is the calculated temperature obtained from equation (12) by letting $D = T_c$ and obtaining values for b_0-b_{19} from table V. The improvement over figure 10 is evident.

To aid in interpreting the 14-term correlation, crossplots of T_c against I, V, and B are presented in figure 13 for the range

$$0.3 \leq I \leq 2.1 \text{ A}$$

$$7 \leq V \leq 20 \text{ kV} \qquad (13)$$

$$0.7 \leq B \leq 3.1 \text{ T}$$

From figure 13(a) it is evident that at high voltage and low magnetic field T_c tends to increase with current until it reaches a maximum. However, for low voltage and high magnetic field T_c is relatively independent of current.

From figure 13(b), T_c tends to increase with voltage. However, for $I = 0.3$ A and $B = 0.7$ T, T_c reaches a maximum and is then relatively independent of V.

From figure 13(c), a high enough value of B will lower T_c. For $V = 20$ kV, T_c is a maximum around 1 T. For lower values of V there may be a maximum of T_c for B less than 1 T.

For the ranges of equation (13) the standard deviation of regression equation (12) is 2.3 to 7.5 percent for T_c.

The 15-term correlation for relative ion density is shown in figure 14 for all the density data (table II). Here the abscissa is the calculated ion density obtained from equation (12) by letting $D = N_c$ and obtaining values for b_0-b_{18} from table VI. The improvement over figure 11 is obvious.

To aid in interpreting the 15-term correlation, crossplots of N_c against I, V, and B are presented in figure 15 for the range

$$0.3 \leq I \leq 1.2 \text{ A}$$

$$7 \leq V \leq 20 \text{ kV} \qquad (14)$$

$$1 \leq B \leq 3 \text{ T}$$

From figure 15(a) it may be seen that N_c is only weakly dependent on current.

According to figure 15(b), relative ion density decreases as voltage increases.

Figure 15(c) shows that at high magnetic fields, N_c increases with B.

For the ranges of equation (14) the standard deviation of regression equation (12) is 8.6 to 62.4 percent for N_c. When it is considered that N_c varies over about seven orders of magnitude, 62.4 percent does not appear serious.

Test section pressure. - The test section pressure could not be read during a plasma discharge because the discharge interfered with the operation of the ion gage. However, with no discharge the pressure was proportional to G and was given by

$$P = 5\times10^{-7} + 1.37\times10^{-4}\ G \qquad (15)$$

where P is the absolute pressure of neutrals in torr, G is the gas flow rate in standard cm^3/sec, and 5×10^{-7} is the background pressure in torr. Hence P varied between 5.1×10^{-5} and 1.3×10^{-4} torr for the 435 runs in table I.

Recommendations for predictions. - Complicated regression equations tend not to make valid predictions for independent variables outside the range of the data used to determine the regression coefficients. Consequently, equation (12) may be used for predictions inside the I-V-B range of the data, but equation (10) or (11), as appropriate, should be used for predictions outside the range.

Current Against Voltage Characteristics of the Plasma Discharge

Figure 16 shows schematics of two typical hydrogen discharge current-voltage (I-V) curves from SUMMA. The lower curve is typical of operation at low gas flow rates and low magnetic field strengths. Increasing the gas flow rate or magnetic field strength caused a change to the upper form. These curves are the same shapes as found previously in the HIP-1 apparatus (ref. 5).

The upper curve shows two distinct plasma modes. At low voltages, the I-V curve was steep; this is a low-resistance mode of the plasma. The curve was almost horizontal at higher voltages, showing a high resistance mode. Voltages near to the peak current and somewhat higher formed an unstable plasma regime. Here the plasma discharge developed a low frequency unstable operating mode in which good data could not be obtained. Operation in the unstable region was avoided.

On the lower curve, the current remained nearly constant as the voltage increased.

The type II curves each had three characteristic voltages as denoted by A, B, and C on figure 16. The first measurable current (~0.01 A) appeared at A. The low and high ends of the unstable operating region are noted as B and C. These 3 voltages were found to vary with the magnetic field strength. For a midplane magnetic field strength of 0.8 T, the values of A, B, and C were approximately 2, 3, and 8 kV, respectively. At 2 T, the values were approximately 4, 12, and 16 kV, respectively. And at 3.4 T the values were approximately 5, 17, and 19 kV, respectively.

The type II curve indicates two plasma "modes," one for voltages less than B and another for those greater than C. The visible flickering and large current changes at low frequencies at voltages between B and C are supporting evidence that "mode" changes were taking place.

In past work in HIP-1 and SUMMA, most efforts had been directed to achieving high ion temperatures. The highest temperatures were always found at the highest voltages and on a type II I-V curve, i.e., in the high resistance mode. With this background, the high resistance mode has been referred to as the ion-heating mode.

In the present study, a number of ion temperatures were taken at voltages as low as 2.3 kV and on both sides of the unstable region of type II curves. The ion temperatures at the low voltages were as low as 18 eV. Unexpectedly, these low temperatures had identically the same current, voltage, magnetic flux density (IVB) dependence as the high temperature data, as was shown. In the light of these findings that all ion temperatures from any of SUMMA's I-V curves have the same IVB dependence, it must be concluded that the same ion heating mechanism is responsible in all plasma modes. It is not proper to consider the high resistance mode as a special ion heating mode.

The average relative ion density in the low resistance mode was calculated to be up to three or four orders of magnitude higher than in the high resistance (high ion temperature) mode. Overall the calculated relative ion densities covered about six orders of magnitude.

Figure 17 shows a few electron temperature data points that had been taken in HIP-1 but not reported (HIP-1 is a plasma fusion apparatus similar to SUMMA but with water-cooled copper magnets). Like the ion temperature and relative ion density results in SUMMA, they show a discontinuity across the unstable plasma operating region. No statistical correlations with current and voltage were made.

Preliminary Absolute Electron Density Results

Two sets of preliminary absolute electron density measurements were made in SUMMA using the laser Thomson scattering diagnostic. These sets will be referred to as Set I, consisting of 19 data points, and Set II, consisting of 28 data points. The data comprising Set I were taken while operating with a different cathode support and floating plate structure than shown in figure 1. Also Set I data were taken at a mirror ratio (1.52) different than the 1.48 mirror ratio of all other data in this report. Set II data were consistent with the spectroscopic data in that these measurements were made while operating with the electrode configuration of figure 1.

The multiple regression analysis applied to the spectroscopic data was used for Set I data with the form given in equation (7). Set I data were taken at a single magnetic flux density of 1.95 T, hence the constant b_3 was not determined. The correlation form then reduces to

$$D = CI^{b_1}V^{b_2} \tag{26}$$

Figure 18 shows the functional relation between the absolute electron density and the voltage and current. The measured electron density ranged from 2.1×10^{11} to 4×10^{12} cm^{-3} and is seen to depend almost linearly on current while having a slight inverse dependence on voltage. The values of V ranged from 4.5 to 22.0 kV and I from 0.14 to 3.0 A for these data.

Similar application of the multiple correlation analysis was not possible for Set II measurements for two reasons: (1) Increased plasma background noise resulted in greater data scatter, and (2) Set II data was restricted almost exclusively to a narrow range in voltage. Table VI shows the range of values for the voltage, current, and absolute density of Set II data. The magnetic field strength was 3.34 T. It should be noted that the 19 kV data point is significant: though there was no detectable background noise at this higher voltage, there was no measurable signal at this operating point either. This indicates electron density may decrease with increasing electrode voltage. Lack of plasma stability excluded operation between 8.5 and 19 kV. Other than the singular data point at 19 kV, the variation in electrode voltage was over too small a range for electron density correlation with respect to this parameter. However, the multiple correlation did give a nearly linear dependence of electron density with respect to current. This agrees with the result of data Set I.

The relative ion density correlation shown in figure 11 was not good, therefore it would be misleading to make direct comparisons between the relative ion density results given in equation (11) and the above absolute electron density results.

CONCLUDING REMARKS

A steady-state hot-ion plasma has been produced and studied in the Lewis SUMMA facility using water-cooled cathodes. Maximum input power was increased by a factor of two relative to values with uncooled cathodes. The studies were made over a range in midplane magnetic flux density from 0.5 to 3.37 T.

A multiple regression analysis was used to determine the functional dependence among the plasma variables current, electrode voltage, midplane magnetic flux density, gas flow, ion temperature, and relative ion density. The ion temperature and relative ion density were measured spectroscopically (the measured ion temperature varied from 18 eV up to 830 eV). The most satisfactory correlations were obtained by correlating ion temperature and relative ion density with current, voltage, and magnetic flux density as independent variables.

A four-term and a multi-term correlation were employed. The four-term correlation was defined as a linear relation between the log of the dependent variable and the logs of the independent variables. The four-term correlation results were compared to previous studies. The multi-term correlation included cross terms through the third order. Statistically insignificant terms in the multi-term correlation were discarded using a backward elimination procedure. The multi-term correlation proved the more satisfactory of the two, but cross plots of the parameters were needed to aid in interpreting the results.

The crossplots from the multi-term correlations were complicated in behavior. However, significant dependences of ion temperature and relative ion density on the dependent variables were noted for certain ranges in these variables. In particular, the relative density increased very rapidly with magnetic field and decreased very rapidly with voltage for high magnetic fields. It increased moderately with current at high magnetic fields. The ion temperature increased with current for high values of voltage and low values of magnetic field. After perhaps passing through a maximum it decreased with magnetic field. It tended to increase with voltage.

Extrapolation outside the range of data should be restricted to the appropriate four-term correlation equations. Multi-term correlations frequently tend not to give valid results outside the range of data.

Preliminary absolute electron density measurements were obtained at two magnetic fields using a Thomson scattering diagnostic. The density varied from 2×10^{11} cm^{-3} to 6.8×10^{12} cm^{-3} and increased linearly with current.

These results could not be compared to the relative ion density data due to the poor fit of the latter using the four-term correlation. In

any case, the relative ion density measurements were not spatially resolved as were the electron density's. Thus, different results could be obtained between the two if the plasma had a pronounced radial variation in density profile which was dependent on a variable such as electrode voltage.

The plasma discharge I-V characteristics were studied. Two modes were believed present: a low resistance mode and a high resistance mode separated by a variable-width unstable region. The ion temperature was revealed to scale identically for both regions. A large change in relative ion density occurred across the unstable region.

APPENDIX - SYMBOLS

A	area of the wide component of H_α
B	midplane magnetic flux density
$\overline{B}$	vector of B
b_0-b_{19}	regression coefficients
C	constant to fit data
D	generalized dependent variable
$\overline{E}$	vector electric field strength
G	total gas flow rate
I	total electric current
I_R	total Rayleigh-scattered light intensity
I_{TH}	total Thompson-scattered light intensity
J	vector current density
K	proportionality constant dependent on total incident radiation power, the scattering length, and the scattering solid angle
N	ion number density
n	principal quantum number
n_e	free electron number density
n_R	number density of Rayleigh scatterers
P	total gas pressure
T	ion temperature
T_e	electron temperature
V	electrode voltage
v	ion velocity
y	distance from line of sight to centerline of test section (see fig. 5)

α	characteristic parameter
θ	scattering angle
λ_o	wavelength of incident laser radiation
λ_D	debye length
σ	cross section
Ω	solid angle scattered into

Subscripts:

c	calculated from regression equation
f	fast
o	observed
R	Rayleigh
TH	Thomson

Special symbols:

$\langle\rangle$	average over velocity space

REFERENCES

1. J. J. Reinmann, M. C. Swanson, C. R. Nichols, S. J. Obloy, L. A. Nagy, and F. J. Brady, NASA Superconducting Magnetic Mirror Facility, Fifth Symposium on Engineering Problems of Fusion Research (Inst. Electrical and Electronics Engrs., New York, 1974), pp. 587-591.

2. J. J. Reinmann, M. R. Lauver, R. W. Patch, S. J. Posta, A. Snyder, and G. W. Englert, IEEE Trans. Plasma Sci., PS-3, 6 (1975).

3. J. J. Reinmann, R. W. Patch, M. R. Lauver, G. W. Englert, and A. Snyder, SUMMA Hot-Ion Plasma Heating Research at NASA Lewis Research Center, NASA TM X-71840, (1975).

4. R. W. Patch and M. R. Lauver, Ion Temperatures in HIP-1 and SUMMA from Charge-Exchange Neutral Optical Emission Spectra, NASA TM X-73471, (1976).

5. J. J. Reinmann, M. R. Lauver, R. W. Patch, R. W. Layman, and A. Snyder, Hot Ion Plasma Production in HIP-1 Using Water-Cooled Hollow Cathodes, NASA TM X-71852, (1975).

6. R. W. Patch, D. E. Voss, J. J. Reinmann, and A. Snyder, Ion and Electron Temperatures in the SUMMA Mirror Device by Emission Spectroscopy, NASA TM X-71635, (1974).

7. W. R. Hess, Phys. Lett., 41A, 66 (1972).

8. D. R. Sigman, J. J. Reinmann, and M. R. Lauver, Parametric Study of Ion Heating in a Burnout-Type Device (HIP-1), NASA TM X-3033, (1974).

9. G. W. Englert, R. W. Patch, and J. J. Reinmann, Abstract 6D17, Bull. Am. Phys. Soc. 20, 1322 (1975).

10. H. W. Drawin and M. Fumelli, Proc. Phys. Soc., 85, 997 (1965).

11. Igor Alexeff, personal communication to R. W. Patch (1976).

12. H. J. Kunze, Plasma Diagnostics, W. Lochte-Holtgreven, ed., (North Holland, Amsterdam, 1968), p. 550.

13. Steven M. Sidik, An Improved Multiple Linear Regression and Data Analysis Computer Program Package, NASA TN D-6770, (1972).

14. N. R. Draper and H. Smith, Applied Regression Analysis, (Wiley, New York, 1966).

15. Henry Margenau, The Mathematics of Physics and Chemistry, (Van Nostrand, New York, 1956), 2nd ed., p. 8.

16. Ralph R. Rudder and David R. Bach, J. Opt. Soc. Am., 58, 1260 (1968).

TABLE I. - RANGE OF VARIABLES COVERED IN 435 RUNS

FOR ION TEMPERATURE AND GAS FLOW RATE

Midplane magnetic flux density, B, T	Number of runs	Gas flow rate, G, Std cm^3/sec		Current, I, A		Electrode voltage, V, kV	
		Minimum	Maximum	Minimum	Maximum	Minimum	Maximum
0.50	8	0.72	0.95	0.83	1.54	11.5	18.3
.67	42	.69	.92	.37	1.92	10.0	18.2
.84	96	.56	.95	.21	2.30	2.3	21.6
1.01	85	.60	.87	.17	2.08	2.5	21.4
1.17	9	.65	.78	.53	1.62	12.4	18.9
1.35	60	.47	.80	.13	1.95	4.7	11.4
1.52	6	.66	.67	.75	.91	14.2	18.4
1.69	28	.45	.78	.17	2.60	5.5	19.5
2.02	15	.45	.45	.19	.84	8.4	19.5
2.36	26	.37	.56	.12	1.90	7.0	19.5
2.70	9	.44	.44	.12	1.36	8.2	17.4
3.04	16	.39	.44	.14	.75	9.3	19.0
3.37	24	.40	.49	.10	1.20	8.0	18.5
3.40	11	.43	.86	.23	2.80	9.0	16.5

TABLE II. - RANGE OF VARIABLES COVERED IN 277 RUNS[a]

FOR RELATIVE ION DENSITY

Midplane magnetic flux density, B, T	Number of runs	Gas flow rate, G_3, Std cm^3/sec		Current, I, A		Electrode voltage, V, kV	
		Minimum	Maximum	Minimum	Maximum	Minimum	Maximum
0.84	74	0.56	0.76	0.21	1.13	2.3	21.6
1.01	58	.60	.76	.17	1.86	2.5	21.4
1.35	36	.47	.64	.13	1.33	4.7	21.4
1.69	20	.45	.60	.17	.72	6.6	19.5
2.02	14	.45	.45	.23	.84	9.3	19.5
2.36	26	.37	.56	.12	1.90	7.0	19.5
2.70	9	.44	.44	.12	1.36	8.2	17.4
3.04	16	.39	.44	.14	.75	9.3	19.0
3.37	24	.40	.49	.10	1.20	8.0	18.5

[a]Subset of 435 runs of table I.

TABLE III. - EXPONENTS FOR ION TEMPERATURE DEPENDENCE

FROM VARIOUS INVESTIGATIONS (SEE EQ. (10))

Investigation	Exponent of current, b_1	Exponent of voltage, b_2	Exponent of magnetic flux density, b_3
Present work	0.27	1.53	-1.05
Ref. 5 (HIP-1)	.3	1.4	-.8
Ref. 4 (SUMMA)	.52	1.64	-1.30
Ref. 4 (HIP-1)	.33	1.50	-.49

TABLE IV. - EXPONENTS FOR RELATIVE ION DENSITY DEPENDENCE FROM TWO INVESTIGATIONS (SEE EQ. (10))

Investigation	Exponent of current, b_1	Exponent of voltage, b_2	Exponent of magnetic flux density, b_3
Present work	1.26	-6.92	5.45
Ref. 5 (HIP-1)	.5	-3.1	3.5

TABLE V. – VALUES OF THE REGRESSION COEFFICIENTS

FOR THREE MULTI-TERM CORRELATIONS

Regression coefficient	Dependent variable	
	T	N
b_0	-0.756418×10^{-1}	0.169203×10^{2}
b_1	----------	$.963319\times10^{0}$
b_2	$.359387\times10^{1}$	$-.299503\times10^{2}$
b_3	$-.386788\times10^{1}$	$.224142\times10^{2}$
b_4	$.288341\times10^{1}$	$-.156171\times10^{2}$
b_5	$.113962\times10^{1}$	$-.858530\times10^{1}$
b_6	----------	----------
b_7	$.273670\times10^{0}$	$-.142072\times10^{1}$
b_8	$-.103754\times10^{1}$	$.199647\times10^{2}$
b_9	$.198407\times10^{1}$	$-.894292\times10^{1}$
b_{10}	$-.145218\times10^{1}$	$.113241\times10^{2}$
b_{11}	$-.720223\times10^{0}$	$.128933\times10^{1}$
b_{12}	----------	$-.231934\times10^{1}$
b_{13}	$.212334\times10^{0}$	----------
b_{14}	----------	----------
b_{15}	----------	$-.966697\times10^{1}$
b_{16}	$-.371880\times10^{1}$	$.115319\times10^{2}$
b_{17}	$-.329355\times10^{0}$	----------
b_{18}	----------	$-.493346\times10^{1}$
b_{19}	$.828916\times10^{0}$	----------

TABLE VI. – RANGE OF VARIABLES COVERED IN SET II

DATA FOR ABSOLUTE ELECTRON DENSITY

Number of data points	Voltage range, kV	Current range, A	Density range, 10^{12} e/cm^3
27	6.4 to 8.5	0.52 to 3.1	0.33 to 6.8
1	19	0.38	Less than 0.1

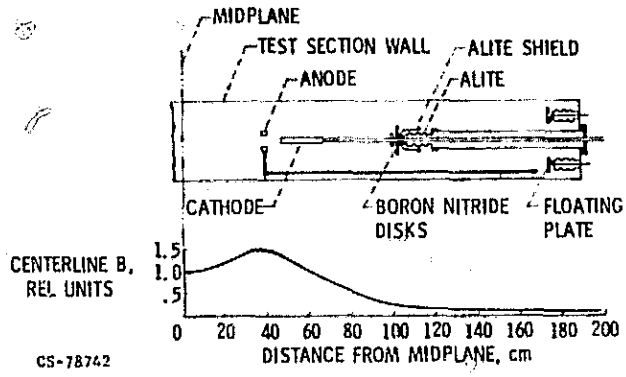

Figure 1. - Summa electrode configuration.

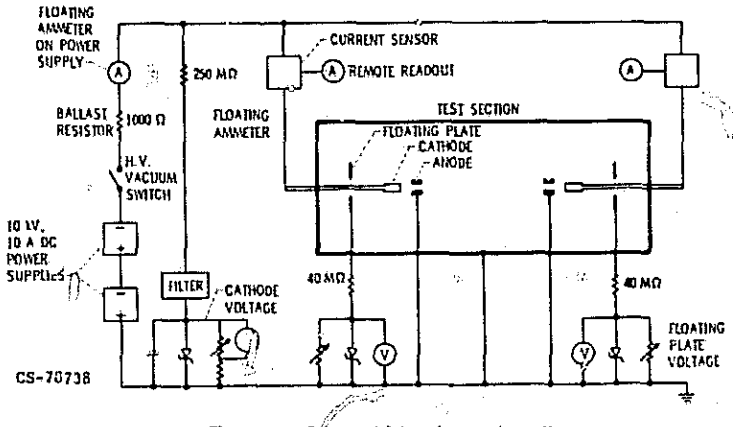

Figure 2. - Summa high voltage schematic.

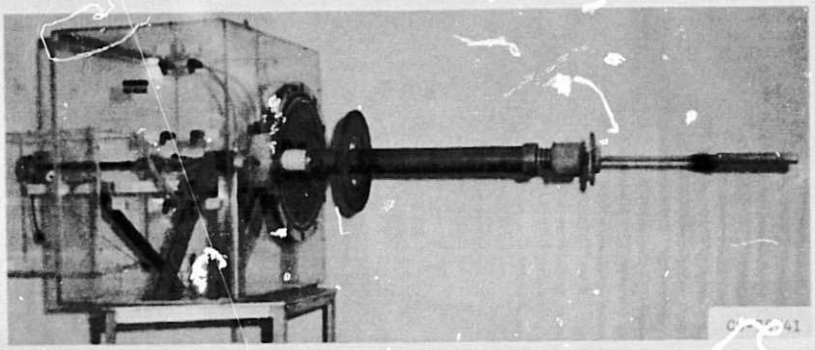

Figure 3. - Summa cathode and end flange assembly.

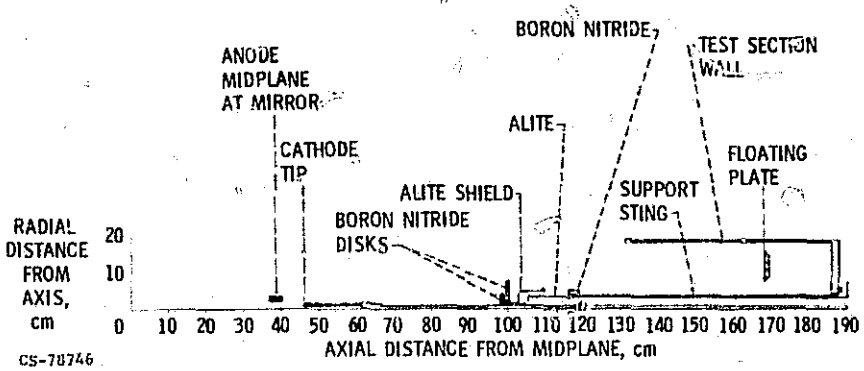

Figure 4. - Summa magnetic field plot showing electrode locations.

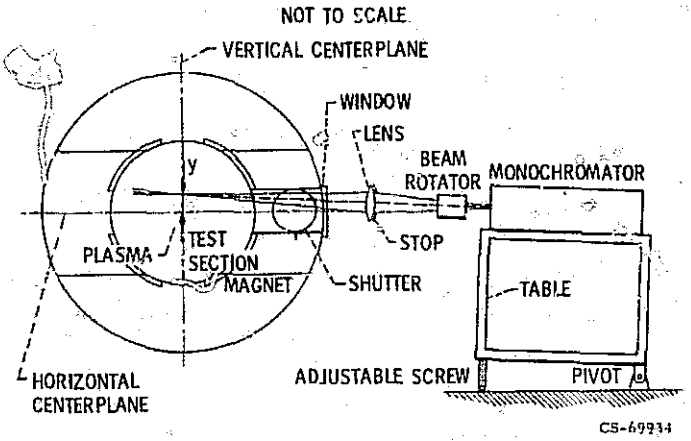

Figure 5. - Apparatus for Doppler broadening and relative ion density measurement.

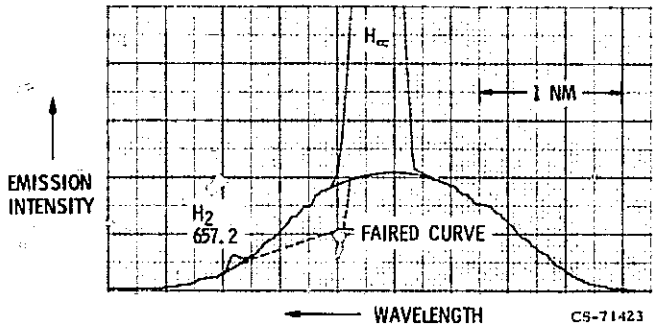

Figure 6. - Typical Balmer-alpha (H_α) line exhibiting wide and narrow components.

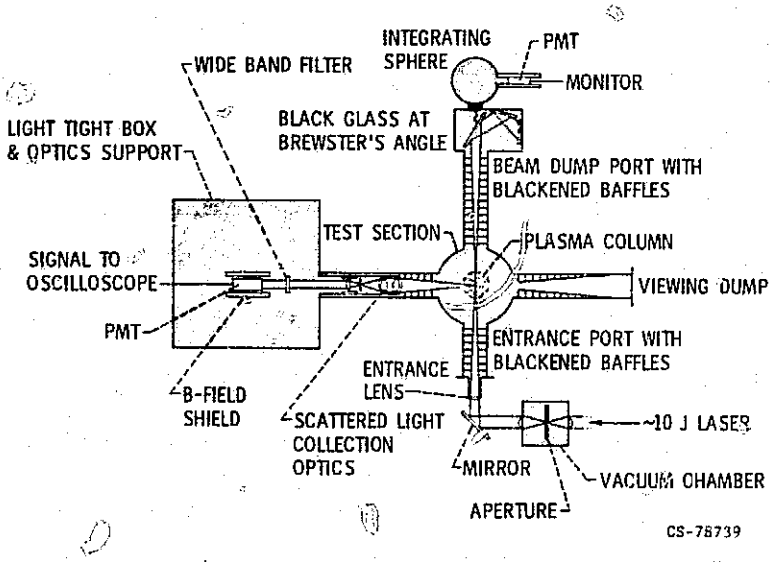

Figure 7. - Laser Thomson scattering apparatus schematic.

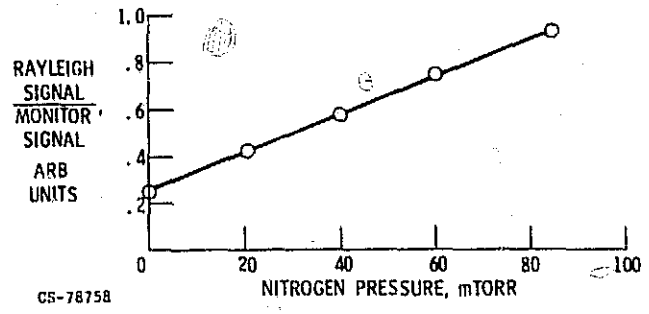

Figure 8. - Rayleigh scattering calibration in dry nitrogen using 0.12 SR solid angle viewing lens.

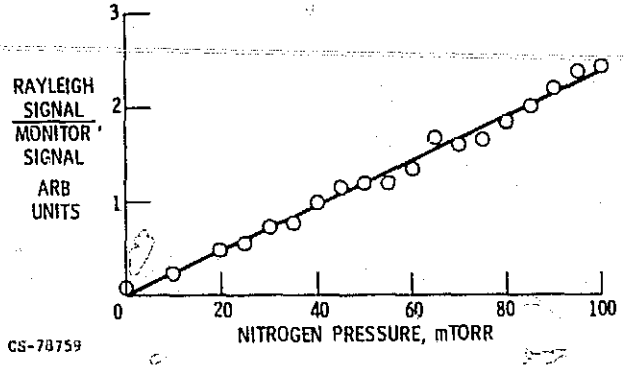

Figure 9. - Rayleigh scattering calibration in dry nitrogen using 0.007 SR solid angle viewing lens.

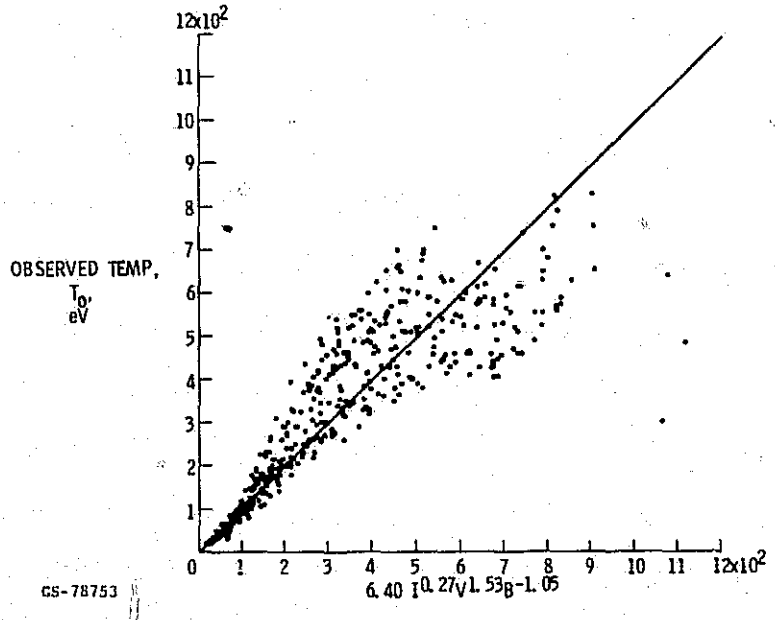

Figure 10. - Ion temperature correlation with 4 terms.

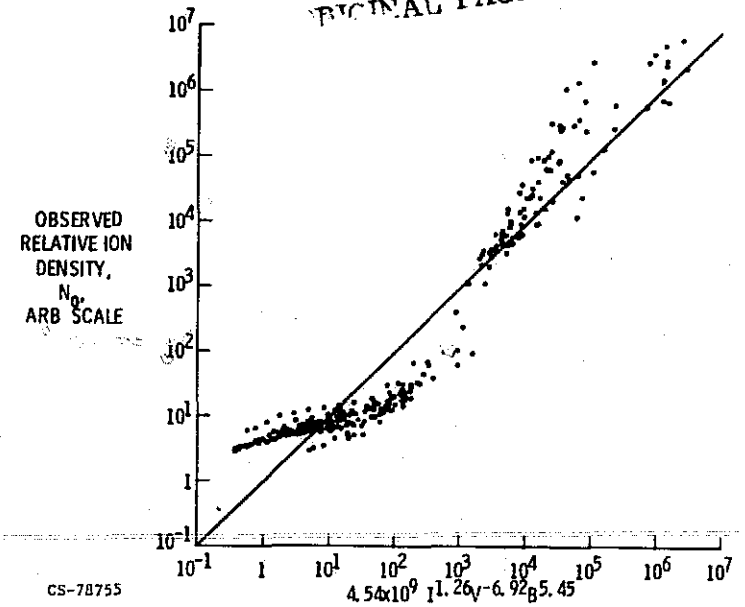

Figure 11. – Relative ion density correlation with 4 terms for all B values.

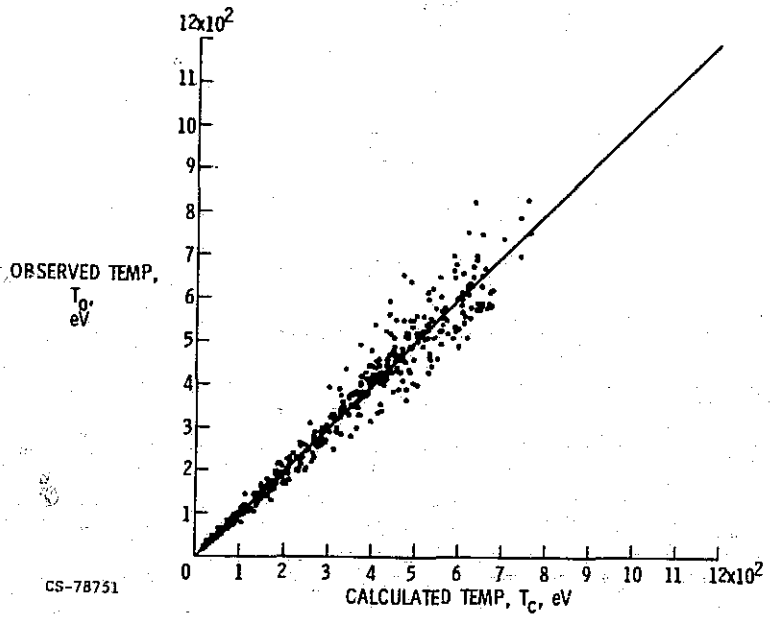

Figure 12. – Ion temperature correlation with 14 terms.

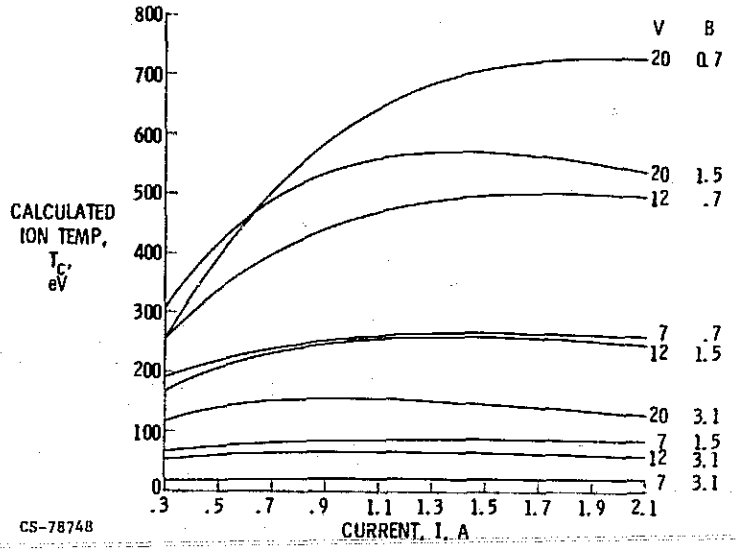

Figure 13(a). - Graph of 14 term regression equation for ion temperature.

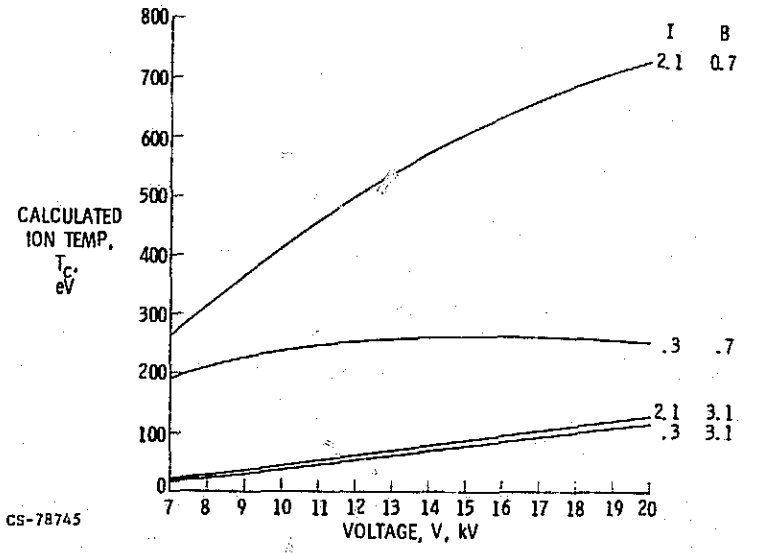

Figure 13(b). - Graph of 14 term regression equation for ion temperature.

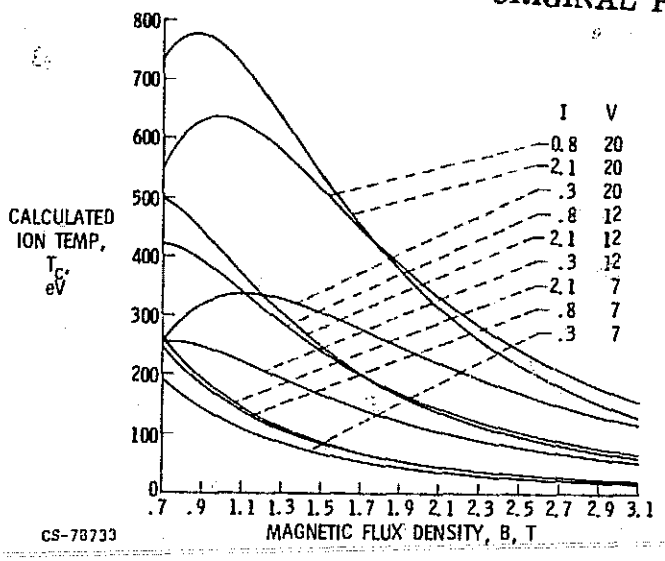

Figure 13(c). - Graph of 14 term regression equation for ion temperature.

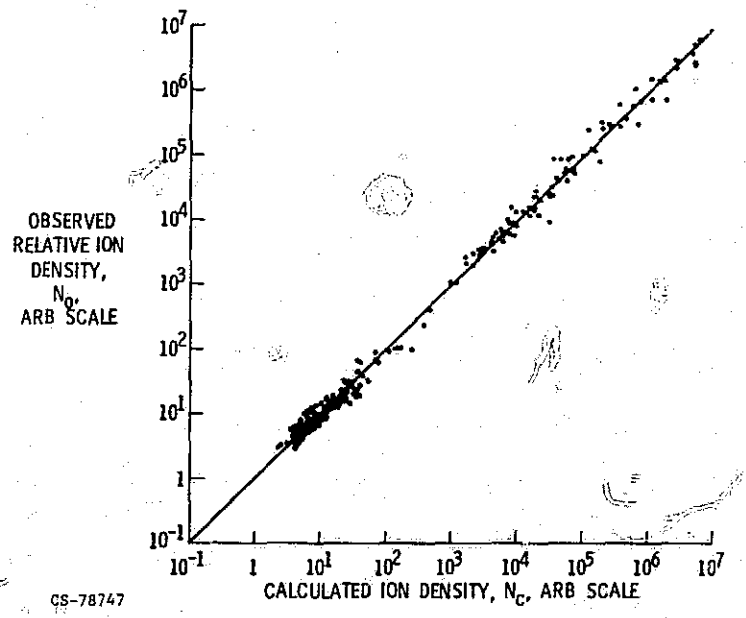

Figure 14. - Relative ion density correlation with 15 terms for all B values.

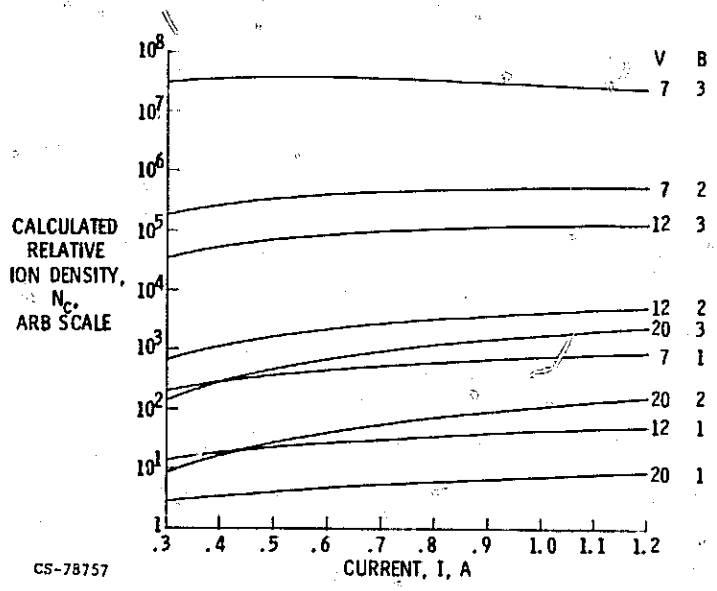

Figure 15(a). - Graph of 15 term regression equation for relative ion density.

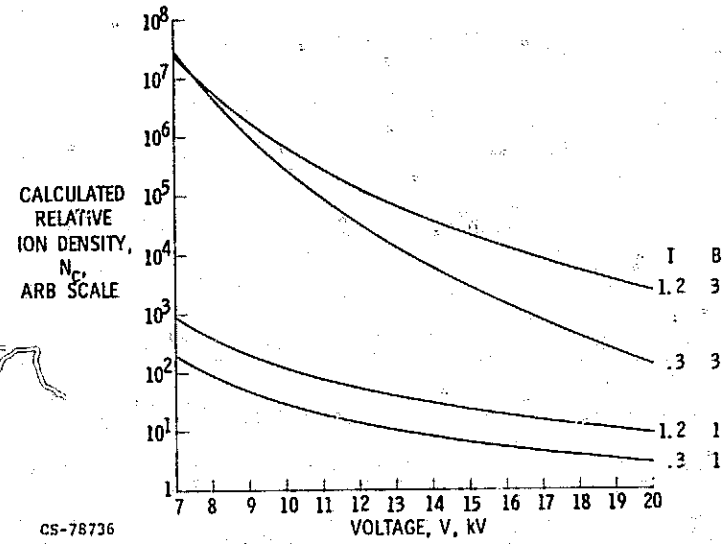

Figure 15(b). - Graph of 15 term regression equation for relative ion density.

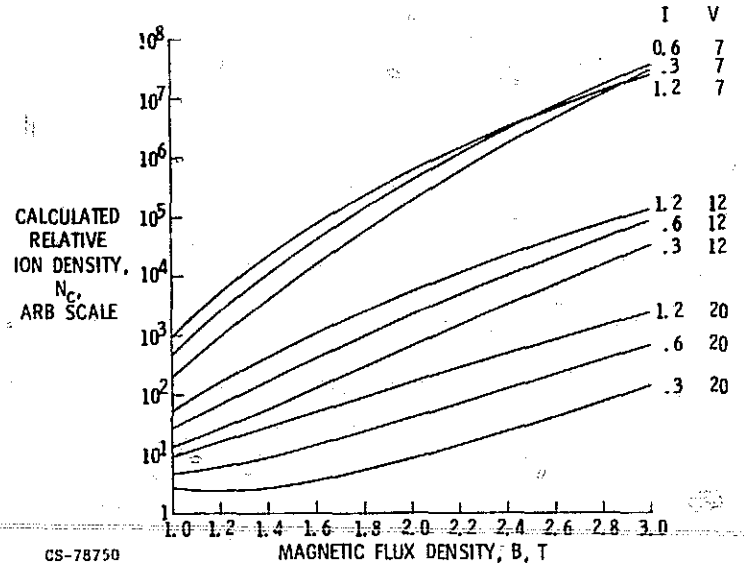

Figure 15(c). - Graph of 15 term regression equation for relative ion density.

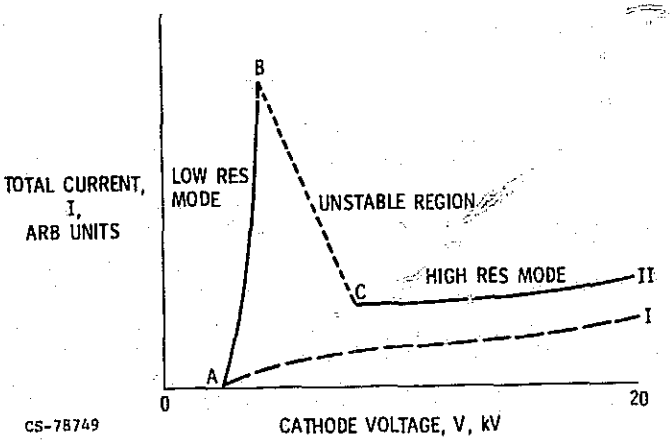

Figure 16. - Representation of typical current versus voltage curves.

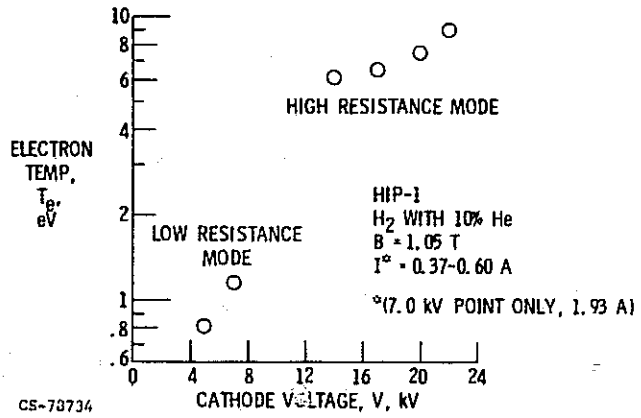

Figure 17.

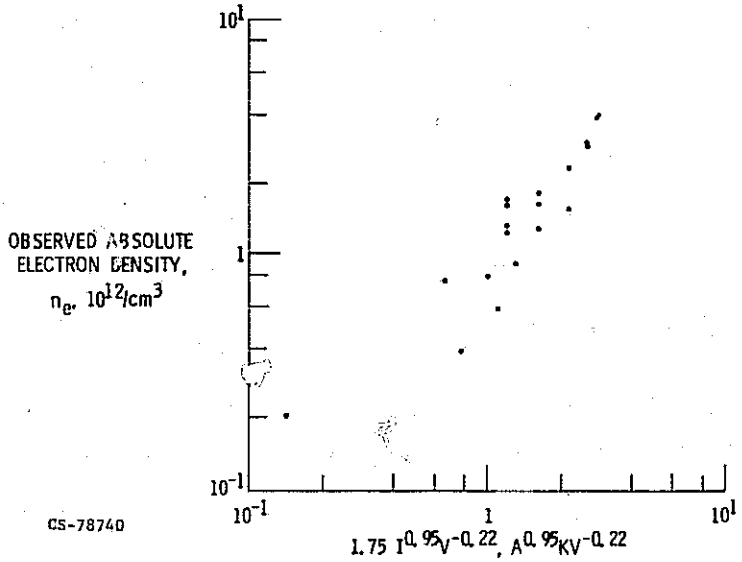

Figure 18. – Absolute electron density correlation with 3 terms.